





# Predicting benthic macroalgal abundance in shallow coastal lagoons from geomorphology and hydrologic flow patterns

Alice F. Besterman <sup>\*,a,b</sup> Karen J. McGlathery, Matthew A. Reidenbach, Patricia L. Wiberg, Michael L. Pace 

Department of Environmental Sciences, University of Virginia, Charlottesville, Virginia

## Abstract

Macroalgae structure coastal ecosystems affecting metabolism, nutrient dynamics, and food webs. Spatially explicit prediction of macroalgal abundance is critical for understanding coastal ecosystems and trajectories. However, models of macroalgal distribution tend to be mechanistic and generalize poorly, or biogeographic and too coarse to use over spatial scales most appropriate to ecosystem research and management (1–100 km<sup>2</sup>). Our objective was to develop spatial distribution models for benthic macroalgae in soft-sediment environments. We compared macroalgal abundance quantified as percent cover, with environmental drivers on 1 ha intertidal flats in a > 900 km<sup>2</sup> lagoon system along the Atlantic Coast of Virginia, U.S.A. Physical drivers of macroalgae (e.g., depth-mediated light availability, exposure to waves) are related to bed morphology. We developed a novel topographic index ( $\tau$ ) to determine whether bed morphology predicts macroalgal abundance. This topographic index described variation in elevation occurring over spatial scales relevant to macroalgae, ranging from smooth to hummocky ( $\tau = 0.01$ – $1.07$ ). Models tested  $\tau$  along with mean elevation, fetch, and water residence time as predictors of macroalgal abundance.  $\tau$ , and the interaction with water residence time, were most strongly related to macroalgal abundance. Hummocky flats accumulated less macroalgae than smoother flats, but exceptions occurred with short residence times. Model error (root mean square error) was low, varying between 8% and 18% across models. These models, based on readily measured physical features, are a useful approach for assessing macroalgal abundance in relation to shoreline hardening, species invasions, sea-level rise, and changing sedimentation affecting coastal ecosystems.

Macroalgae structure coastal ecosystems through density-dependent controls on metabolism (McGlathery et al. 2001; Hardison et al. 2011), nutrient dynamics (Tyler et al. 2003; Gonzalez et al. 2013), biodiversity, and food webs (Valiela et al. 1997; Thomsen et al. 2009; Green and Fong 2016; Umanzor et al. 2019). Accurate and spatially explicit estimates of macroalgal abundance are important for understanding coastal ecosystems and predicting future trajectories. Existing approaches include mechanistic models of macroalgal dynamics developed for individual bays (tens of km<sup>2</sup>) (Salomonsen et al. 1997; Thomsen et al. 2006; Nejrup and Pedersen 2010), and large-scale, low-resolution biogeographic models (thousands of km<sup>2</sup>) (Martínez et al. 2012; Snickars et al. 2014; Kotta

et al. 2019). Methods are less well developed for macroalgal prediction over intermediate spatial domains. Predictive models of macroalgae based on easily measured variables on the order of 1–1000 km<sup>2</sup> domains are needed.

Mechanistic approaches focus on statistical or mathematical prediction of macroalgae in relation to drivers that directly affect growth and abundance. Macroalgal populations are related to nutrients, light availability, and herbivory (Burkpile and Hay 2006; McGlathery et al. 2007; Thomsen and McGlathery 2007; Nejrup and Pedersen 2010). Accumulation also depends on substrate availability (Thomsen and McGlathery 2005; Kollars et al. 2016; Krueger-Hadfield et al. 2016). Macroalgae need hard substratum for spore settlement and recruitment, but some algae can grow indefinitely once they become detached from hard substratum, such as species in the Gracilariales (Kain(Jones) and Destombe 1995; Guillemain et al. 2008; Krueger-Hadfield et al. 2016). Mechanism-based predictions are complicated by interactions among drivers that lead to site-specific macroalgal responses. Physical factors interact with nutrient enrichment, leading to nonlinear macroalgal responses to nutrients (Valiela et al. 1997; Cloern 2001). For example, increasing water residence time in

\*Correspondence: abesterman@woodwellclimate.org

Additional Supporting Information may be found in the online version of this article.

<sup>a</sup>Present address: Woodwell Climate Research Center, Falmouth, Massachusetts, USA

<sup>b</sup>Present address: Buzzards Bay Coalition, New Bedford, Massachusetts, USA

the presence of high nutrient loading results in a parabolic macroalgal biomass response, with increasing residence time associated with higher biomass up to a threshold above which biomass decreases due to self-shading in thick macroalgal accumulations (Valiela et al. 1997; McGlathery et al. 2007; Swaney et al. 2008). Limited substrate for fixation may reduce macroalgal abundance in comparison to other estuaries even when nutrient, light, and grazer conditions are suitable. These mechanistic approaches do not facilitate prediction of macroalgal abundance at larger scales because they require accurate field measurements, and may produce nonlinear, site-specific macroalgal responses.

Biogeographic models focus on patterns of macroalgal diversity and abundance across regional scales. Species distribution modeling (SDM) approaches have been used in this context, which make use of correlative patterns between an organism and environmental gradients to predict abundance (Snickars et al. 2014; Kotta et al. 2019). Patterns between macroalgal abundance and depth, slope, wave exposure, substrate, salinity, and temperature have been identified using these approaches (Thomsen et al. 2006; Snickars et al. 2014; Kotta et al. 2019). These exercises mostly focus on perennial macroalgae in subtidal or rocky intertidal habitats (Holmes et al. 2008; Martínez et al. 2012; Snickars et al. 2014; Kotta et al. 2019), so that with few exceptions (Thomsen et al. 2006; Martins et al. 2007), shallow soft-sediment environments and bloom-forming macroalgae have not been considered. SDM approaches overcome the difficulty of predicting macroalgal responses from interacting, mechanistic drivers. However, these biogeographic patterns are too coarse to make spatially explicit predictions within a site, or between sites, unless they vary significantly along a gradient such as temperature.

In this study, we focus on predicting macroalgae on intertidal flats in shallow coastal lagoons. To recruit and develop into the adult life cycle stage, all macroalgae require hard substrate, which is limited in soft-sediment coastal lagoons (Thomsen and McGlathery 2005; Krueger-Hadfield et al. 2016; Lees et al. 2018). Macroalgae can be found fixed by a holdfast to hard substrate when it is available in soft-sediments (Krueger-Hadfield et al. 2016); such as on oyster reefs and shell fragments (Thomsen et al. 2006). However, in coastal lagoons macroalgae tend to be free-floating or anchored by tubes of the polychaete *Diopatra cuprea* on subtidal and intertidal flats (McGlathery et al. 2001, 2012). *Diopatra cuprea* is a tube-forming polychaete that facilitates macroalgae on soft-sediment flats by incorporating thalli into its tube, anchoring macroalgae to the sediment (Thomsen and McGlathery 2005; Kollars et al. 2016). Where *D. cuprea* are abundant macroalgae can form thick, benthic mats extending over hundreds of meters (Besterman and Pace 2018). However, *D. cuprea* are not easily mapped in these environments without intensive field effort, thus are not useful for predictive spatial modeling. Mapping hydrologic flow variables with an SDM approach may be a solution because *D. cuprea* are found in fine sands

(Gosner 1971; Luckenbach 1986), and sediment grain size is driven by hydrologic conditions (Wiberg et al. 2015). For spatial domains on the order of thousands of m<sup>2</sup> hydrologic flow is more readily mapped than *D. cuprea* or macroalgae, and is independently related to macroalgal abundance.

Hydrologic flow variables affect the growth and stability of macroalgae on intertidal flats. Water residence time, which correlates with macroalgal retention (McGlathery et al. 2007), and salinity and temperature (Swaney et al. 2008), can vary between less than 5 and more than 2000 h (Wiberg et al. 2015). Water currents affect the distribution (Flindt et al. 1997), and productivity of macroalgae on intertidal flats (Jørgensen and Revsbech 1985; Sand-Jensen and Frost-Christensen 1999). Slow moving waters result in thicker diffusive boundary layers, which have negative effects on production due to decreased mass transport of oxygen, carbon dioxide, and dissolved nutrients across the thallus surface. Waves disturb and mobilize macroalgae, decreasing abundance (Krause-Jensen et al. 2007; Martínez et al. 2012; Snickars et al. 2014), or contribute, along with currents, to transport and deposition of macroalgae on intertidal flats (Lanari and Copertino 2017). In coastal lagoons, water residence time and wave energy are related to water depth, wind fetch, and topography which differ significantly over short distances (Fagherazzi et al. 2007; McGlathery et al. 2013; Wiberg et al. 2015; Ganju et al. 2017). Hydrologic and geomorphic variables may provide integrative metrics that capture the effects of multiple environmental drivers on macroalgal abundance (Holmes et al. 2008), while exhibiting strong gradients useful for testing.

In this study, we test combinations of hydrologic and geomorphic variables as predictors of macroalgal distributions using an SDM approach. Coastal lagoons are useful systems to test these variables as macroalgal predictors because they exhibit broad gradients over short distances (hundreds of meters). We performed these tests in a system where grazing is not a significant control on biomass (Thomsen and McGlathery 2007), and nutrients are low (Anderson et al. 1997), suggesting a dominant role for physical variables driving macroalgal distribution. We focused on intertidal flats because they often accumulate large masses (100 s g m<sup>-2</sup>) of macroalgae (Thomsen et al. 2006; Lanari and Copertino 2017; Besterman and Pace 2018), but are less well studied than other coastal habitats such as coral reefs and seagrass meadows. Tidal flats are abundant, covering at least 127,900 km<sup>2</sup> of earth surface (Murray et al. 2019). Tidal flats exhibit significant variability in bed elevation across their surface inclusive of oyster reefs (Volaric et al. 2018), tidal channels, bedforms (Fagherazzi et al. 2013), and biofilm-driven ridges and runnels (Weerman et al. 2010), all of which may all affect macroalgal distribution.

We were particularly interested in testing models using only remotely sensed geomorphic variables (in contrast to those using field measurement-intensive variables), because high resolution bathymetric and digital elevation maps are

increasingly available for coastal areas. Predictive models that require only bathymetric or digital elevation data would provide significant opportunities for macroalgal research over large spatial scales and among coastal ecosystems. In systems where other variables are deemed important (e.g., nutrients, temperature), these physical models may serve as a baseline for other variables to be added. We tested measures of mudflat topography varying over 1–20 m in spatial scale as predictors of macroalgal abundance and distribution. We focus on mudflat topography for a few reasons. Topographic relief affects macroalgal accumulation on rocky intertidal shorelines (Cox et al. 2017), so may be relevant on tidal flats. Topographic relief exhibits a wide gradient across tidal flats. Also, the scale of topographic features seemed promising for resolving macroalgal abundance at the hectare scale. Mudflat topographic features are likely driven by larger-scale hydrologic patterns, and also modify flow patterns locally (Fagherazzi et al. 2013; McGlathery et al. 2013; Wiberg et al. 2015, 2019). As a result, these topographic features may serve as an integrative metric of multiple drivers of macroalgal abundance.

We had two specific goals for this research. First, to develop a metric to quantify mudflat topography on intertidal flats and to identify drivers of these formations. Second, to compare statistical linear models predicting macroalgal abundance and distribution using readily measured or modeled geomorphic (mudflat topography, elevation) and hydrologic (water residence time, fetch) variables (Table 1). These goals supported our overarching objective to identify predictive models of macroalgae using physical variables.

## Methods

### Study area

This study was conducted in the Virginia Coast Reserve (VCR) Long-Term Ecological Research Site, a 110 km stretch of protected coastline including shallow lagoons, marshes, barrier islands, and tidal flats (Figs. 1, 2). The barrier islands form a semi-enclosed system of 14 coastal lagoons having distinct tidal, depth, and mixing properties, with oceanic exchange occurring through narrow inlets between the islands (Safak et al. 2015). Lagoon beds are largely underlain by shallow flats with average depth about 1 m below mean sea level (Safak et al. 2015). The VCR is a soft-sediment environment (Wiberg et al. 2015), and most back-barrier tidal flats are muddy. The patchy distribution of ecosystems landward of the islands creates a seascape with highly variable fetch, water residence time, sediment grain size, vegetation structure, and elevation (Fig. 1). The watersheds that feed the coastal lagoons are small and primarily covered with forests and agriculture, with large expanses of intact riparian vegetation at the land–water interface (Stanhope et al. 2009; Anderson et al. 2010; Giordano et al. 2011). Low freshwater input results in salinities near seawater strength across the

lagoons. Average summertime temperatures across the bays are within 2°C (Wiberg pers. comm).

Watershed nutrient input to the lagoon is low, and among the lowest reported for similar lagoon systems around the world (Anderson et al. 1997; McGlathery et al. 2001). Two lagoons have been regularly sampled since 1992 (areas sampled shown on map: Supporting Information Fig. S1). The average daily dissolved inorganic nitrogen concentration between 2007 and 2017 was 4.1  $\mu\text{mol L}^{-1}$ , SD = 3.7  $\mu\text{mol L}^{-1}$  (McGlathery and Christian 2018). There is no significant difference in dissolved inorganic nitrogen concentrations across a horizontal gradient from the mainland to the islands, or between lagoons (McGlathery and Christian 2018). Experimental nitrogen enrichments of macroalgae did not enhance growth rates, despite increased nitrogen uptake (Thomsen and McGlathery 2007). The rapid turnover of nutrients in lagoon sediment supports the nitrogen demand of benthic macroalgal mats in this system (McGlathery et al. 2001; Tyler et al. 2003). With benthic nutrient turnover supplying nitrogen to macroalgae, and low nitrogen loading from the mainland, dissolved nitrogen concentrations do not drive abundance patterns of macroalgae across the VCR.

Macroalgae are generally distributed throughout intertidal and subtidal ecosystems (Thomsen et al. 2006; Gulbransen et al. 2012). In the VCR, mats of macroalgae typically grow over 10–40% of exposed area on intertidal flats with 18 g dw  $\text{m}^{-2}$  average biomass, and maxima > 300 g dw  $\text{m}^{-2}$  (Besterman and Pace 2018). Macroalgal mats are distributed in patches on tidal flats, and range in size from < 0.25  $\text{m}^2$  to

**Table 1.** Names and parameters for all models tested.

Model group	Model name	Parameters
Percent clay models		
—	Clay-A	RT
—	Clay-B	fet
—	Clay-C	fet + RT
$\tau$ models		
—	SEM- $\tau$ -A	Clay
—	SEM- $\tau$ -B	Clay + fet + RT
Macroalgal models		
Full data set		
	Full-A	$\tau_d$ + elev
	Full-B	$\tau_d$ *RT
	Full-C	$\tau_d$ *RT + fet
	Full-D	$\tau_d$ *RT + elev
Less than 30% only		
	Low cover-A	$\tau_d$ + elev
	Low cover-B	$\tau_d$ *RT
	Low cover-C	$\tau_d$ *RT + fet
	Low cover-D	$\tau_d$ *RT + elev

$\tau_c$ , continuous mudflat topography;  $\tau_d$ , discrete mudflat topography; elev, elevation; fet, fetch; RT, residence time.

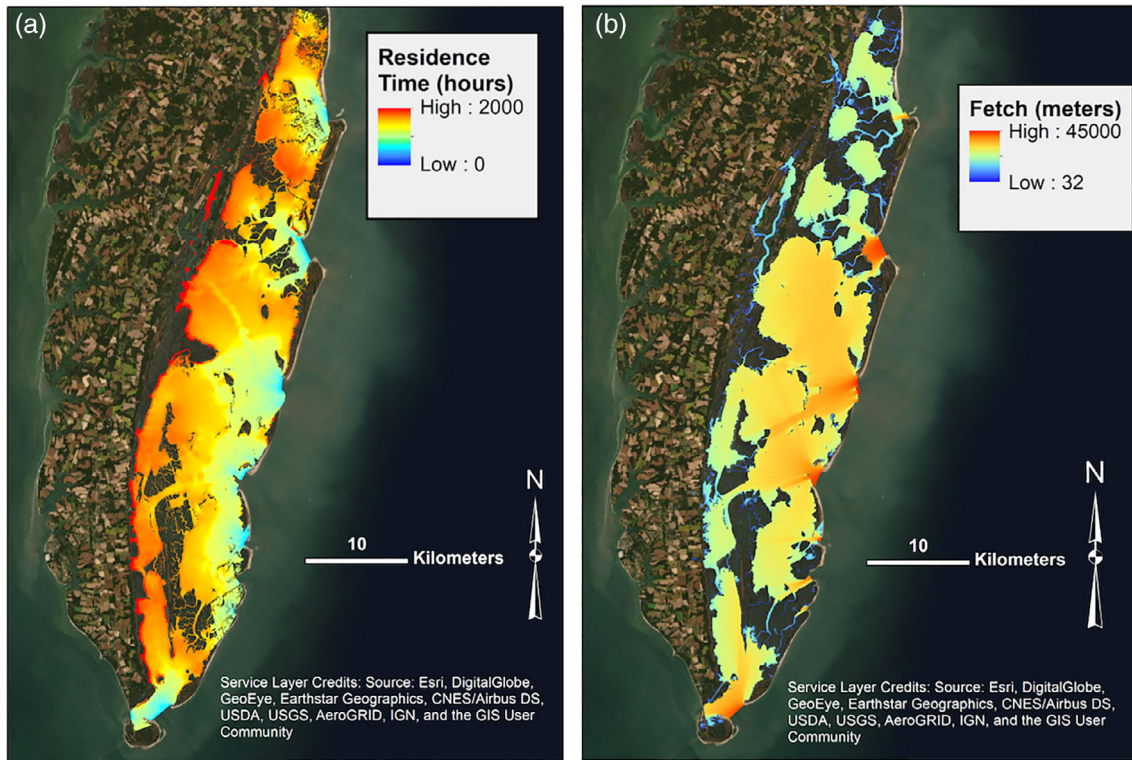


**Fig. 1.** Water residence time and fetch in the Virginia Coast Reserve LTER. Maps showing (a) the distribution of log-transformed water residence time in hours (left), and (b) log-transformed fetch in meters (right).

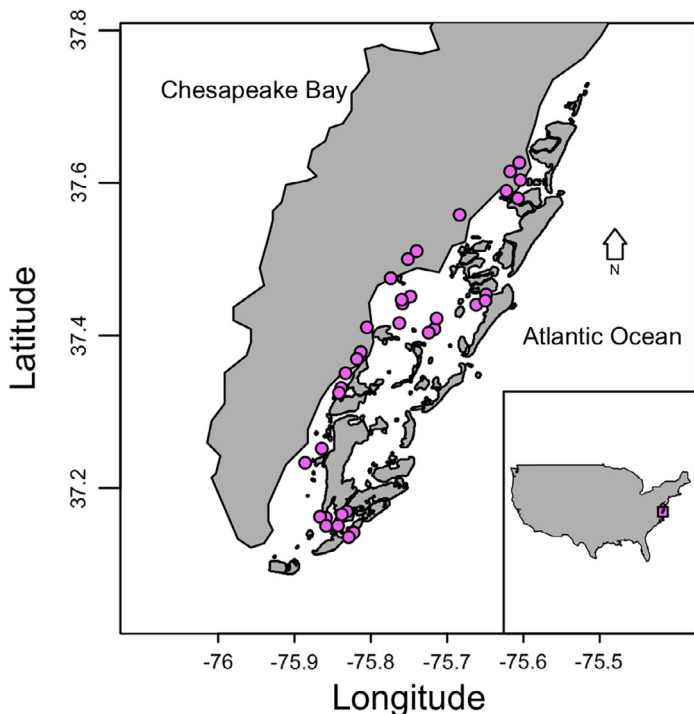


**Fig. 2.** Map of study system and sites. Main map shows the Virginia Coast Reserve (VCR) LTER, inset shows position of VCR relative to United States. Violet dots are study sites. One site was just north of the map boundary in the larger map.

hundreds of  $m^2$ . Macroalgal abundance on intertidal flats in the VCR is low to moderate compared with other temperate estuaries (Lyons et al. 2009; Nejrup and Pedersen 2010; Byers et al. 2012; Sutula et al. 2014).

The dominant macroalga in both intertidal and subtidal habitats (Thomsen et al. 2005; Gulbransen et al. 2012), *Agarophyton vermiculophyllum* (previously referred to as *Gracilaria vermiculophylla*) (Gurgel et al. 2018) is an invasive species originating from east Asia (Krueger-Hadfield et al. 2017). In the VCR, *A. vermiculophyllum* dominates on tidal flats, representing > 60% of macroalgal biomass (Thomsen et al. 2006; Besterman and Pace 2018). However, there is still moderate macroalgal diversity in the VCR, with other native species including multiple *Ulva* spp. comprising secondary dominants in terms of biomass. *A. vermiculophyllum* can tolerate desiccation better than native species, promoting its stability and accumulation (Thomsen and McGlathery 2007; Thomsen et al. 2009). Macroalgae, and *A. vermiculophyllum* especially, is stabilized on flats by a facilitative interaction with *Diopatra cuprea* (Thomsen and McGlathery 2005). *D. cuprea* incorporates macroalgae into its tube, anchoring thalli to the flat. As a result, the distribution of *D. cuprea* partially controls the distribution of macroalgae. *Agarophyton vermiculophyllum* is little grazed (Thomsen and McGlathery 2007), so top-down control of biomass is negligible. Macroalgal diversity and ecology

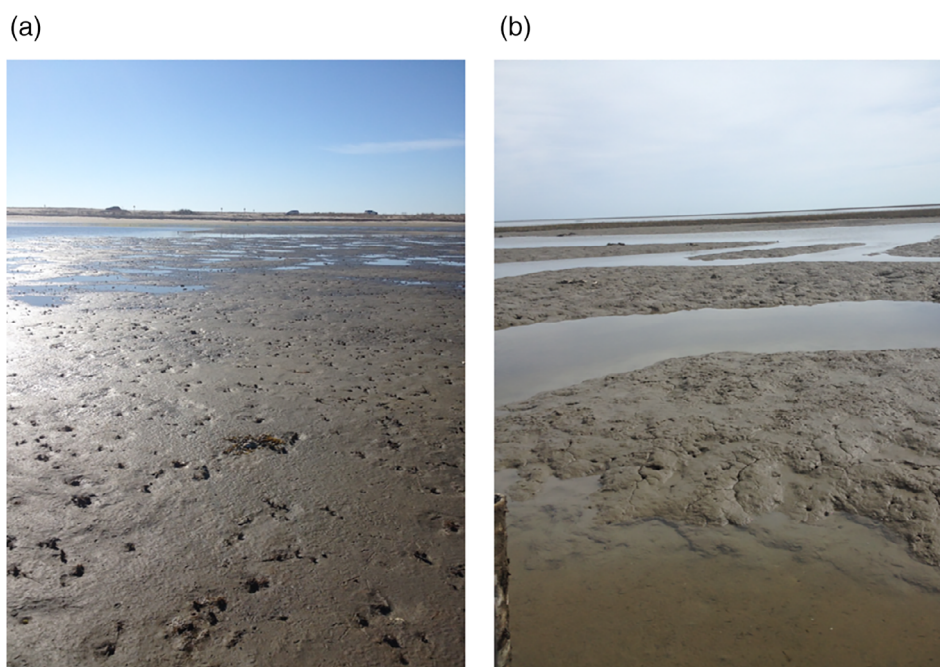


**Fig. 3.** Photographs of representative (a) smooth and (b) hummocky mudflats in the Virginia Coast Reserve LTER.

(Thomsen et al. 2006; Besterman and Pace 2018) and the *A. vermiculophyllum* invasion (Thomsen et al. 2005; Gulbransen et al. 2012; Krueger-Hadfield et al. 2017) are described in more detail elsewhere.

#### Site selection

We selected 36 intertidal flats distributed across 10 of the lagoons within the VCR and one additional lagoon just north of the VCR boundary (Fig. 2). The selected intertidal flats

covered the entire east–west gradient from near the barrier islands to near the mainland. The flats varied between: highly exposed and sheltered, dominantly sandy to dominantly muddy, and closer to and farther from an inlet. Intertidal flats in the VCR exhibit significant variability in mudflat topography, with some featuring a hummock-hollow morphology (series of higher-elevation “hummocks” with lower elevation “hollows” between them) while others appeared entirely smooth (Figs. 3, 4). Each site was sampled over a 120 m

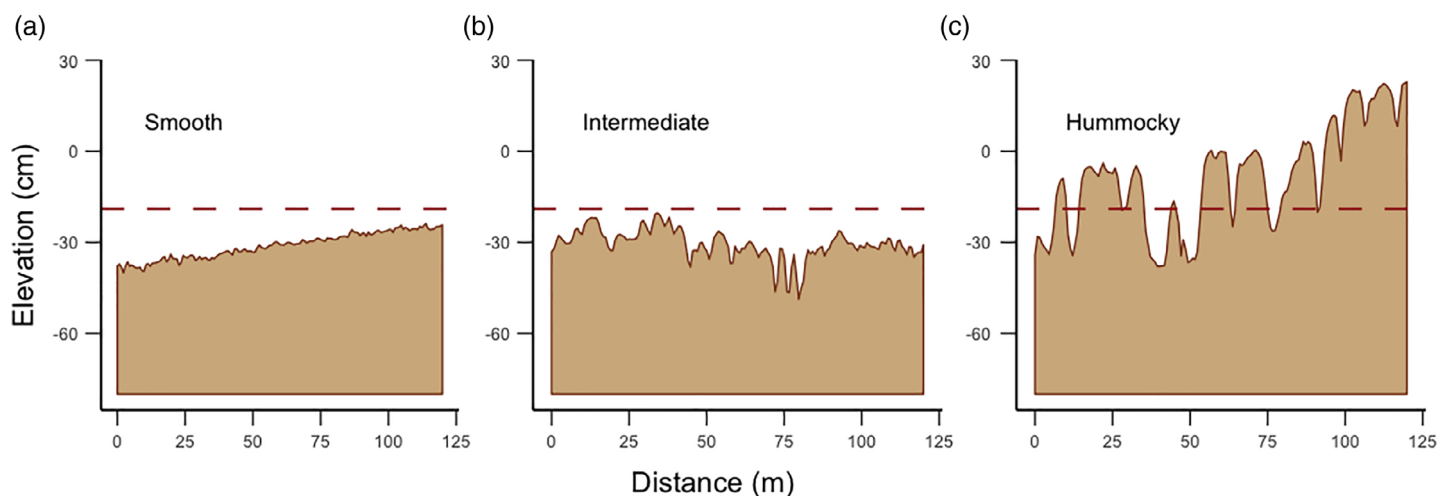


**Fig. 4.** Elevation profiles for three representative transects from a smooth, intermediate, and hummocky flat. Each profile is a single 120 m transect from a flat. Elevation is cm relative to mean sea level and the dashed line is mean elevation across all intertidal flats. Panel (a) smooth mudflat topography, this site had the lowest topographic index variable, (b) intermediate site, (c) hummocky site, this site had the largest topographic index variable.

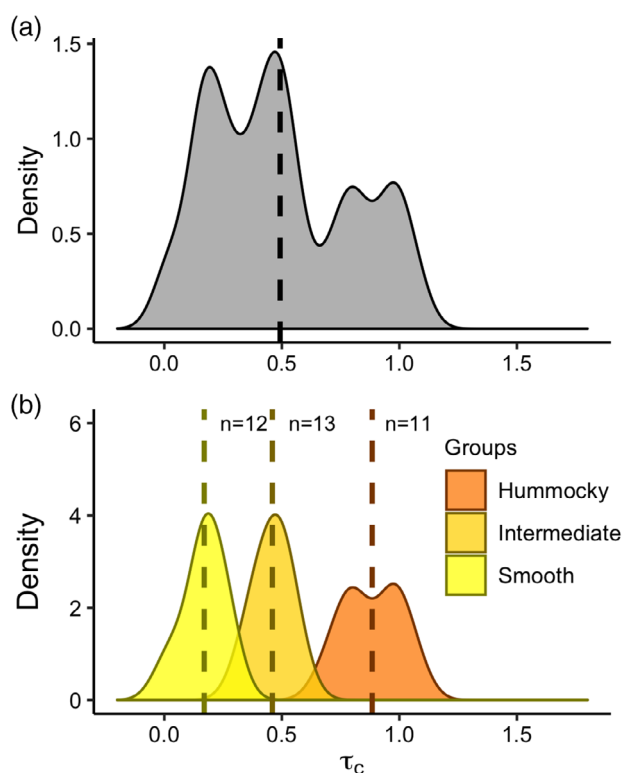


**Fig. 5.** Distribution  $\tau$  (mudflat topography) across 36 intertidal flats. Top panel (a) shows kernel density distribution of unitless  $\tau$ , dashed line = median. Bottom panel (b) shows density distribution of each group, dashed lines = group means, and  $n$  = sample size shown on figure. Smoother on both plots equals 0.0669.

diameter circular plot. In some cases, these circular sampling plots included marsh, lagoon, or channel because the shape and size of the flat could not fit an entire 1.13 ha plot. Field sampling was conducted along a 120 m transect running across the plot diameter. For each flat, we determined percent cover as well as a suite of possible predictor variables as detailed below.

#### Fetch, water residence time, and sediment grain size

Water residence times for the 36 sampled flats were extracted from a hydrodynamic model for the entire VCR (Safak et al. 2015, Fig. 1). This approach estimated residence by tracking neutrally buoyant tracers released from a 300-m-resolution grid of locations in the hydrodynamic model; further detail about the method can be found in Safak et al. (2015). Particle-tracking residence time was estimated for 30 low-tide releases and 30 high-tide releases; here we used the averaged values from the high-tide releases, as has been done elsewhere (Safak et al. 2015; Wiberg et al. 2015), because these produced the largest gradient in particle-tracking residence time across the lagoons, and included intertidal areas. Fetch distances were modeled for the entire VCR based on wind data from 2014 to 2015 and scripts developed for ArcGIS

9.0 (Ferguson 2018). Fetch values for the 36 sites examined in this study were extracted from this data set (Fig. 1). Both fetch and residence time were highly skewed, so variables were  $\log_{10}$ -transformed, which effectively normalized the distributions.

In order to characterize sediment size distributions, we used modified 60 cm<sup>3</sup> syringes to collect four, 2-cm deep sediment cores from each site at randomly determined distances along the sampled transect. Samples were stored in whirl-pak bags, and kept at 4°C until analysis. Organic matter was removed from sediment samples prior to analysis using a hydrogen peroxide digestion, and remaining supernatant was removed. We did not acidify samples since the VCR does not have significant carbonates in sediments (Greiner et al. 2013). Sodium hexametaphosphate was added as a dispersant, then samples were run on a Beckman-Coulter BLS 13320 Laser Diffraction Particle Size Analyzer in duplicate. The averaged particle size distribution was used in subsequent analyses. We calculated the mean and median particle sizes, as well as the percent clay. Clay particles were considered to be those smaller than 4  $\mu$ m.

To understand the relationship between flow-related variables and sediment grain size for study sites, we compared three regression models (Table 1). Previous work has shown that residence time is a strong predictor of grain size properties (Wiberg et al. 2015). Since we were most interested in clay content due to its cohesive properties, because cohesion likely impacted the formation of hummocks, we focused on predicting percent clay. We were also interested if fetch predicted percent clay on intertidal flats. The three regression models predicting percent clay were: a simple regression with only residence time (Clay-A), a simple regression using only fetch (Clay-B), and a multiple regression model using both fetch and residence time (Clay-C) (Table 1). The untransformed data met model assumptions for predicting clay content. We compared these statistical models with Akaike information criterion (AIC) corrected for small sample sizes (AIC<sub>C</sub>), to determine which model was best for predicting clay content on intertidal flats (Zuur et al. 2009; Burnham et al. 2011). This approach is used for statistical model selection by standardizing goodness-of-fit statistics across models, so that models using different predictor variables can be directly ranked and compared (Burnham and Anderson 1998). The best model has the lowest AIC<sub>C</sub> score, and differences of less than four indicate models have similar predictive power (Burnham and Anderson 1998; Arnold 2010).

#### Mudflat topography and elevation

Elevation data for study flats were extracted from a high-resolution Light Detection and Ranging (LiDAR)-based 2015 digital elevation model (DEM) with a horizontal resolution of 0.7 m and vertical root mean square error (RMSE) for non-vegetated terrain of 0.06 m (Dewberry 2016). Data were converted to meters above mean sea level (m above msl). To

**Table 2.** Elevation, amplitude, and percent clay statistics for  $\tau$  groups. Superscript letters indicate significant differences in elevation and percent clay among sites determined by ANOVA and Tukey HSD post hoc tests. Amplitude is distance of hummock height, hollow depth—a measure not applicable (NA) to smooth sites because these sites did not have hummocks. Clay content is the percent of sediment grains  $< 4 \mu\text{m}$  at the site.

Variable	Statistic	Tidal flat topography groups ( $\tau$ )		
		Smooth	Intermediate	Hummocky
	<i>n</i>	12	13	11
Elevation (m above msl)	<i>Range</i>	−0.60 to −0.02	−0.37 to 0.36	−0.18 to 0.00
	<i>Mean</i>	−0.33 <sup>a</sup>	−0.14 <sup>b</sup>	−0.11 <sup>b</sup>
	<i>SD</i>	0.14	0.23	0.09
Amplitude (m)	<i>Range</i>	NA	0.05–0.09	0.09–0.21
	<i>Mean</i>	NA	0.06	0.13
	<i>SD</i>	NA	0.01	0.04
Clay content (%)	<i>Mean</i>	12.53 <sup>a</sup>	14.75 <sup>a</sup>	23.42 <sup>b</sup>
	<i>SD</i>	8.40	7.26	4.83

estimate elevation for each intertidal flat studied, we extracted elevations from four 120 m transects oriented N-S, E-W, NW-SE, and NE-SW. In total, this produced approximately 640 elevation measurements per site. Fewer points were collected from some sites because residual standing water remained on the tidal flat at low tide. Because LiDAR cannot penetrate water to measure bed elevation, the data were actually reflecting the water surface. This effect is referred to as “hydroflattening,” and these points were removed prior to analysis. Due to significant skewness in the elevation data, central tendency statistics (mean, median) poorly characterized site elevation patterns (Supporting Information Fig. S2). To solve this problem, elevation for each flat was described using the 75<sup>th</sup> percentile of the sampled data, which better characterized the distribution.

To predict macroalgal abundance, we sought an index that could describe the topographic variability of each tidal flat with a single statistical metric, and could compare tidal flats across the smooth to hummocky topographic gradient. Similar metrics such as rugosity (the ratio of the contoured horizontal distance to the idealized horizontal distance) have been developed for describing coral reef topography, but these were not ideal for our purposes (Dahl 1973; Rogers et al. 2018). Some tidal flats in the VCR exhibit low frequency (one or two features per 120 m transect) but large amplitude (0.3 m or greater) topography, while others exhibit high frequency (~20 features per 120 m transect) but smaller amplitude (0.10 m or less) topography. As a result, tidal flats with few extreme topographic features could result in similar rugosity measurements to tidal flats with more moderate but higher frequency topographies. Related metrics such as the root-mean-square approach measure the deviation between an idealized

sinusoidal topographic profile, with the actual depth profile (Rogers et al. 2018). This approach could result in similar metrics for a flat with irregular hummocks that deviated from a sinusoidal curve, and a smooth flat that did not exhibit hummocks at all (Rogers et al. 2018). Since these topographic metrics were not suitable for the observed mudflat features, we developed a novel topographic metric.

The index variable ( $\tau$ ) was developed to characterize the mudflat topography across the flats. First, we fit a 25-point (17.5 m) moving average for each transect on each site, and calculated the residuals between the raw elevation data and the moving average (Supporting Information Fig. S3). Again, due to skewness in the data, we used the 75<sup>th</sup> percentile of the absolute value of the residuals to characterize the intertidal flat mudflat topography (Supporting Information Fig. S4). Finally, across sites  $\tau$  was right skewed, so we  $\log_{10}$ -transformed the values to produce the  $\tau$  index statistic. More detail about the method and an example calculation are provided in the Supporting Information.

We explored the shape of the  $\tau$  distribution across all sites using a kernel density plot (R Core Team 2019) (Fig. 5). The distribution exhibited multiple peaks, indicating  $\tau$  may have breakpoints (Fig. 5). We used a cluster analysis to investigate  $\tau$  classification. A  $k$ -means method was used with the Hartigan and Wong algorithm, as described in the documentation for function “*kmeans*” in package “*stats*” in R (Hartigan and Wong 1979; R Core Team 2019). The results of the cluster analysis were used to classify sites as having smooth, intermediate, or hummocky  $\tau$  (Fig. 5). In subsequent tests, we tested  $\tau$  as both a continuous variable ( $\tau_c = 0.01$ – $1.07$ ), and as a discrete variable ( $\tau_d = \text{smooth, intermediate, or hummocky}$ ) using the assignments from the cluster analysis.

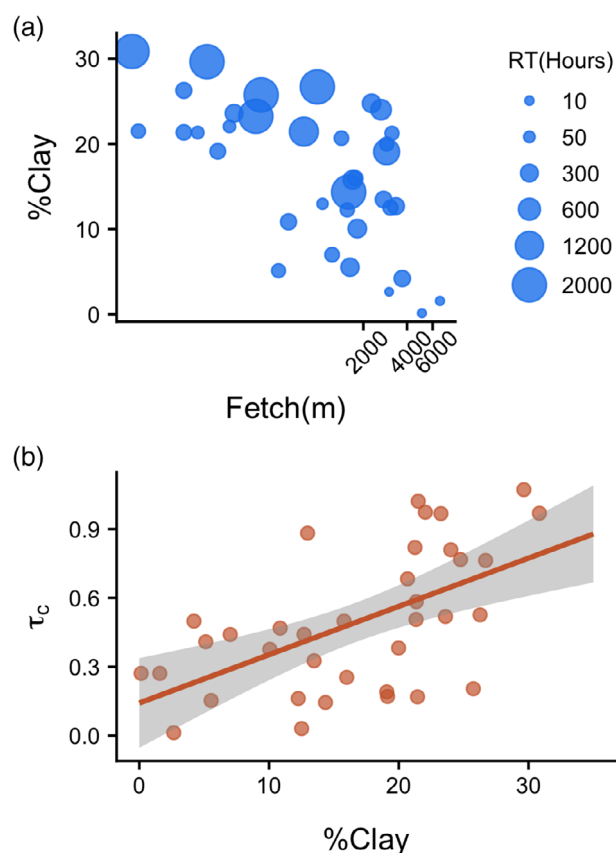


**Fig. 6.** (a) Relationship between percent clay, residence time, and fetch (top panel). Water residence time (RT), and fetch predict percent clay on intertidal flats. (b) Relationship between percent clay and mudflat topography (bottom panel). Prediction of  $\tau_c$  by clay content, with model fit line and 95% confidence interval (bottom).  $\tau_c$  = mudflat topography index as a unitless, continuous variable, where low values are smooth flats and high values have high heterogeneous, “hummocky” mudflat topography. Fetch is log-transformed.

We tested the differences in percent clay, and elevation, across  $\tau_d$  and  $\tau_c$  using ANOVA with Tukey HSD post hoc tests, as well as linear regression. We checked that these tests met all assumptions. We calculated the amplitude of the hummock-hollow elevation patterns on hummocky and intermediate sites. To do this, we first calculated the 90<sup>th</sup> percentile of the absolute-value residuals calculated from the moving average. The 90<sup>th</sup> percentile was a threshold for the clearest peaks and troughs across the intertidal flats. This value was an approximation of mudflat topography amplitude.

Using structural equation modeling (SEM), we explored the causal relationships among flow variables, sediment grain size, and  $\tau$  (Table 1). The goal was to determine if flow variables had a direct effect on  $\tau$ , or only indirect by controlling sediment grain size. Full methods describing our approach are in the Supporting Information, but briefly, SEM is a method of testing multiple models simultaneously that have a structural relationship (Supporting Information) (Grace et al. 2010;

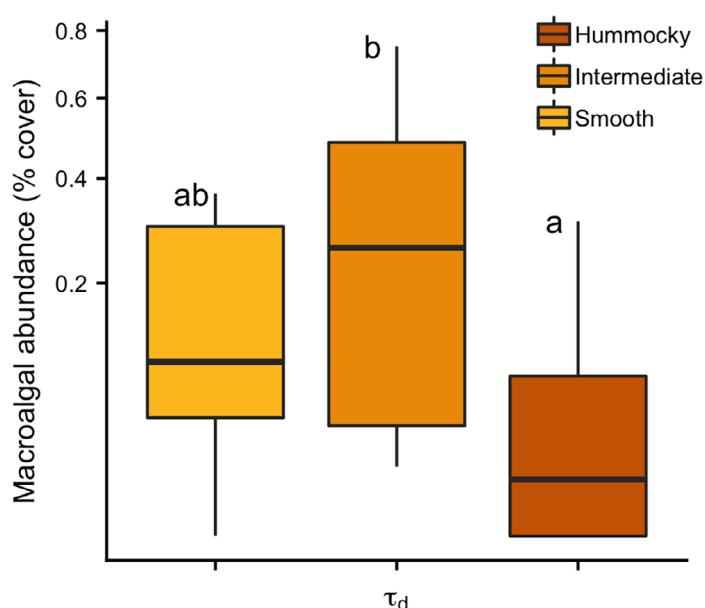


**Fig. 7.** Box-and-whisker plots for macroalgal abundance as percent cover by  $\tau_d$  groups (discrete mudflat topography). Macroalgal abundance shown on sqrt-transformed axis. Legend shows  $\tau_d$  groups with lightest color corresponding with smooth flats, middle shade showing intermediate flats, and the darkest color showing hummocky flats. Significant differences are shown with the letters, where intermediate flats differed from hummocky flats, but smooth flats were similar to both hummocky and intermediate flats. Upper and lower box boundaries show the 75<sup>th</sup> and 25<sup>th</sup> percentiles of the distribution, and whiskers extend to the most distant value on either end of the distribution, excluding outliers (1.5 times the interquartile range). There was one outlier in the hummocky group, not shown on this figure.

Lefcheck 2016). This enables testing the effects of indirect and direct variables on a response.

### Macroalgal cover

At each site, we quantified macroalgal abundance as cover by visually scanning the 1.13 ha mudflat plot from the edge, and estimating percent cover. Researchers practiced estimating cover by visual scans at a training mudflat (1 ha plot, not included in the data presented here). We estimated cover by visually scanning from the plot edge, then validated the scan estimates by standard transect sampling using a 0.25 m<sup>2</sup> quadrat at 40 sampling points. Thereafter, each researcher ( $n = 3$ ) estimated the percent cover at a site, and we averaged the estimates to produce the abundance estimate used for analyses. This approach was used in order to facilitate rapid data collection. This was necessary to complete all sampling within a short enough time frame that we could exclude seasonal effects on macroalgal abundance. We collected biomass samples from randomly determined points along the sampled transect to characterize the macroalgal community, using a 0.0625 m<sup>2</sup> quadrat ( $n = 8$  per site). We identified collected macroalgal samples to functional group (red filamentous, green filamentous, green foliose), and to species when

**Table 3.** Model selection for linear prediction of macroalgal abundance. Model names in the first column correspond with those in Table 1. Low cover models are abbreviated as just “low” here.  $AIC_C$  = AIC corrected for small sample sizes, and  $\Delta AIC_C$  = difference between a model and the best-fit model.  $\tau_{int}$  = intermediate mudflat topography,  $\tau_{sm}$  = smooth mudflat topography, RT = water residence time, elev = elevation, and fet = fetch. Validation columns show the correlation (Corr) and root mean square error (RMSE) between predicted and observed for previously collected data (years 2015, 2016). In 2015, we compared three sites, and in 2016 four sites. Comparisons were not possible with low cover models. (–).

	Model terms and parameters						$\Delta AIC_C$	$R^2$	Validation		
	$\tau_{int}$	$\tau_{sm}$	RT	$\tau_{int} * RT$	$\tau_{sm} * RT$	Elev			Fet	Corr	RMSE
Full-B	0.55	-0.70	-0.23	-0.14	0.36			0	0.43	0.87	0.08
Full-D	0.68	-0.72	-0.20	-0.20	0.33	-0.35		0.04	0.48	0.91	0.07
Full-C	0.80	-0.73	-0.21	-0.25	0.36		0.09	1.40	0.46	0.92	0.06
Full-A	0.28	0.08				-0.38		2.06	0.29	0.93	0.07
Low-D	-0.77	-0.58	-0.13	0.36	0.23	-0.50		0	0.68	–	–
Low-A	0.12	-0.03				-0.55		3.83	0.43	–	–
Low-B	-0.62	-0.55	-0.17	0.29	0.28			9.68	0.45	–	–
Low-C	-0.58	-0.59	-0.15	0.28	0.28		0.08	10.19	0.53	–	–

possible. We used the percent cover data collected in the field to build and assess models that predicted macroalgae from environmental variables.

### Linear models to predict macroalgal abundance

We used multiple linear regression to test models predicting macroalgal abundance. Different combinations of

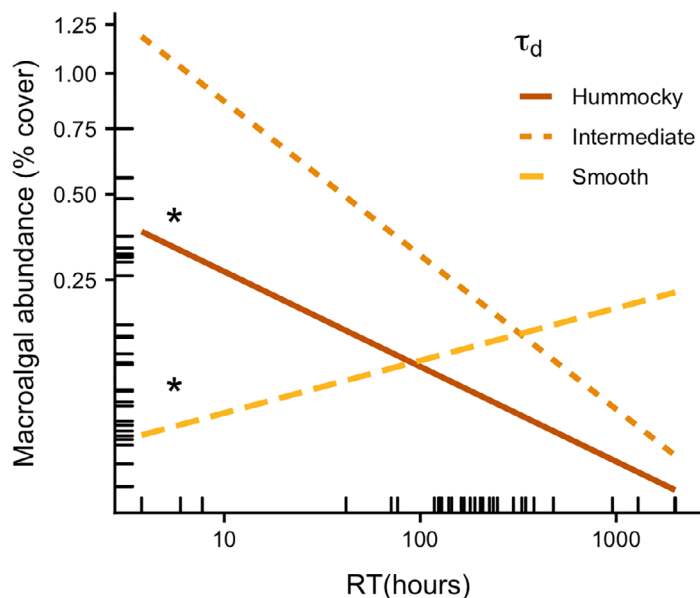


**Fig. 8.** Effect of interactions between RT (water residence time) and  $\tau_d$  (discrete mudflat topography) for prediction of macroalgal abundance as percent cover. Figure shows fitted models for macroalgal abundance predicted by RT separated by  $\tau_d$  groups. X-axis is  $\log_{10}$ -transformed and y-axis is  $\sqrt{\text{transformed}}$ . Legend shows color and line type for each group, where the dark solid line is hummocky, the short dash and medium shade is intermediate  $\tau_d$ , and the lightest shade and long dash is smooth flats. Hummocky and smooth slopes were significant, indicated by \*.

$\tau$ , fetch, residence time, elevation, and interactions among these variables were again used as predictors (Table 1). We initially explored interactions between both fetch and mudflat topography, and residence time and mudflat topography. Since the residence time-mudflat topography interaction was stronger, and the literature supports residence time as a predictor of macroalgae, subsequent model formulations used this interaction instead of fetch-mudflat topography. The main effect of fetch as an independent variable was still tested in models. Fetch and water residence time were  $\log_{10}$ -transformed to meet model assumptions for predicting macroalgal abundance. We tested models using both the continuous ( $\tau_c$ ) and discrete ( $\tau_d$ ) metrics of mudflat topography, and compared which specification was a better predictor.

In the data exploration process, we observed significant heteroscedasticity; specifically, that when macroalgal abundance as cover was  $> 30\%$ , model skill decreased sharply. Consequently, we explored a reduced data set (hereafter, Low Cover models) using the same set of models, and contrasted these results with the full data set (hereafter, Full models) (Table 1). The reduced data set had 26 observations, and corrected the heteroscedasticity.

The four best models, based on  $AIC_C$ ,  $R^2$ , and residual plots, for both the full and reduced data sets were selected for further evaluation. We also explored interaction effects by testing regressions on data subsets to identify over what ranges patterns were significant. To validate the linear models, we compared model predictions against previously collected macroalgal cover data from three of the study sites in 2015, and four of the study sites in 2016 (Fig. 3). Although cover was compared on the same tidal flats for multiple years, these seven spring estimates were reasonably independent because macroalgae senesce in late summer and can detach and advect off flats during storms (McGlathery et al. 2001). We calculated the correlation between the predicted data, and observed data

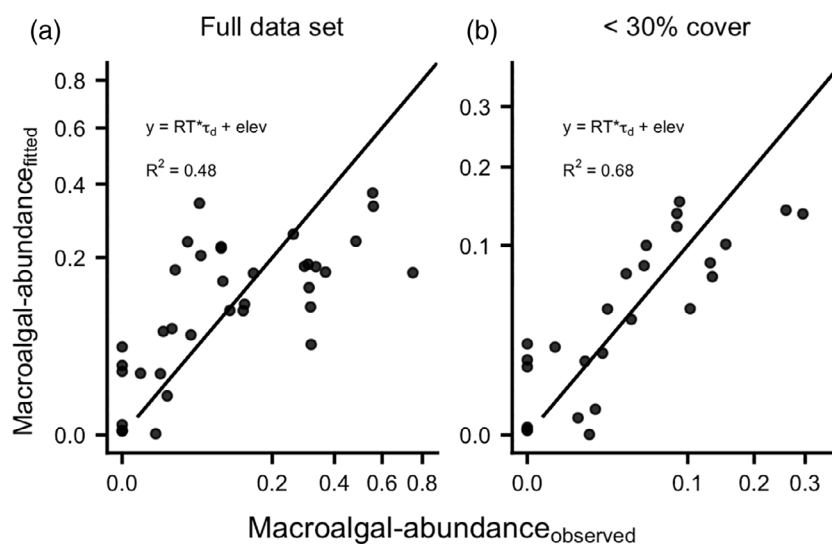


**Fig. 9.** Model fit for best (a) full data set model, and (b) low cover model where macroalgal abundance < 30%. Plots show observed vs. predicted data; line shows a slope of 1 for reference, and axes are square-root transformed. Each plot shows model equation where elev = elevation,  $\tau_d$  = mudflat topography, RT = water residence time. Interactions are symbolized using (\*).

from 2015 and 2016, and also RMSE. The best four models were selected for reporting. Additional details on statistical techniques are provided in the Supporting Information.

## Results

### Fetch, water residence time, and sediment grain size

Fetch and residence time both varied over three orders of magnitude across sites in the VCR. Fetch ranged between 51 and 6700 m, with an average of 900 m (based on the log-normal distribution). Residence time (resolution ~ 7 ha) range was 4 h to over 2000 h. Average residence time was 200 h (based on the log-normal distribution). Fetch and residence time were not strongly correlated ( $r = -0.33$ ). Locations with short residence time were closer to inlets, while long residence time sites were closer to the mainland (Fig. 1a).

Across sites percent clay (particles < 4  $\mu\text{m}$ ) ranged between 0.14% and 31%. On average, intertidal flats in the VCR contained 17%, SD = 8.3% clay (Table 2). Clay-C, the model including fetch and residence time best explained the variation in clay fraction on the flats ( $F_{2,33} = 15.7$ ,  $R^2 = 0.49$ ,  $p < 0.001$ ) (Fig. 6). Delta-AIC<sub>C</sub> scores for Clay-A and Clay-B were both greater than 4. Percent clay decreased with increasing fetch ( $\beta_{\text{fetch}} = -0.002$ ), and increased with longer residence times ( $\beta_{\text{residence}} = 0.004$ ).

### Mudflat topography and elevation

The mudflat topographic index  $\tau_c$  varied over 100-fold (Table 2). At the low end ( $\tau_c = 0.01$ ), mudflat topography was gently sloping, sandy, without any apparent topographic relief (Fig. 4a). The most hummocky (i.e., largest  $\tau_c$  values) site

( $\tau_c = 1.07$ ) was a sheltered, semi-enclosed mudflat where distance between hummock peaks and hollow troughs were consistently 30–40 cm (Fig. 4c). The  $k$ -means cluster analysis grouped the  $\tau_c$  data into a hummocky group ( $n = 11$ ), a smooth group ( $n = 12$ ), and an intermediate group ( $n = 13$ ) (Table 2; Fig. 5).

The hummocky group had clear hummock-hollow formations across the flat platform; on average the amplitude was 0.13 m (calculated using 90<sup>th</sup> percentile elevations, described above), and mean  $\tau_c = 0.88$  (Fig. 4; Table 2). At some sites, the hummock-hollow formations were regular and nearly parallel with perpendicular orientation to the main channel (Supporting Information Fig. S5a). In other cases, the formations were more dendritic, without a dominant orientation (Supporting Information Fig. S5b). A third case existed where the flat was incised by larger channels, with less branching, producing a more stochastic elevation pattern across the flat platform (Supporting Information Fig. S5c). For the hummocky flats exhibiting perpendicular or dendritic formations, the distance between hummock peaks ranged from about 10–20 m. Flats in the smooth group did not exhibit these larger scale formations; however, they were not perfectly smooth either. Smooth flats tended to have high frequency, low relief variations in elevation, that were within LiDAR data error range (< 6 cm) (Figs. 3, 4). The patterning on the intermediate flats was less clear and followed at least three patterns. In the first case, flats appeared to have regular hummock formations; but these formations were lower relief than those on the hummocky sites, so they did not fall into the hummocky category (Supporting Information Fig. S6a). In the second case, the tidal flat exhibited a sharp transition between

hummocky and smooth mudflat topography (Supporting Information Fig. S6b). These transitions appeared to correspond with the presence of oyster reefs. In a third case, intermediate flats exhibited randomly located high or low points that were not large enough or frequent enough to classify the flat as hummocky, but too large for the flat to be classified as smooth (Supporting Information Fig. S6c).

Clay significantly differed among  $\tau_d$  groups ( $F_{2,33} = 7.6$ ,  $p = 0.002$ ). Hummocky flats had 23% clay on average, with higher clay content by 9% ( $p = 0.013$ ), and 11% ( $p = 0.002$ ) than intermediate or smooth sites, respectively (Table 2). Intermediate and smooth flats did not differ in clay content (Table 2). Percent clay was linearly related to  $\tau_c$  ( $F_{1,34} = 16.5$ ,  $\beta_{\text{clay}} = 0.02$ ,  $p < 0.001$ ,  $R^2 = 0.33$ ) (Fig. 6). The Clay-models indicated both fetch and residence time were important, so we used an SEM test to determine whether fetch and residence time were directly related to  $\tau$ , or only indirectly through the effects on sediment grain sizes deposited on flats (percent clay) (Supporting Information). The SEM revealed that residence time and fetch were important for predicting percent clay, and percent clay directly predicted  $\tau$  (Fig. 6). But residence time and fetch were only indirectly related to  $\tau$  through percent clay, without any direct effects (Supporting Information). We checked residuals for the SEM tests, and the models met all assumptions (Supporting Information).

Across all sites, the mean elevation was  $-0.19$  m,  $SD = 0.19$  m above msl. Elevation ranged between  $-0.6$  and  $0.4$  m above msl (Table 2). Elevation differed among topographic groups ( $F_{2,33} = 6.4$ ,  $p = 0.004$ ). Smooth sites were  $0.2$  m lower in elevation on average than intermediate ( $p = 0.017$ ) or hummocky ( $p = 0.006$ ) sites. Intermediate and hummocky sites were similar to each other in elevation, both about  $-0.1$  m above msl (Table 2).

### Macroalgal cover

The dominant macroalga was *Agarophyton vermiculophyllum*, comprising 68% of macroalgae on intertidal flats on average. Other important macroalgae were filamentous and foliose *Ulva* spp. In addition, various species of red, green, and brown macroalgae were observed in samples in small amounts, including *Bryopsis* sp., *Ceramium* spp., *Leathesia* sp., and *Agardhiella* sp. Macroalgal cover on intertidal flats was 16% ( $SD = 20\%$ ) on average. Overall, cover ranged between 0% and 75%, and demonstrated a right-skewed distribution with a median value of 8.7% cover. Macroalgae were present on 83% of intertidal flats in the VCR, and 70% of intertidal flats had at least 2% macroalgal cover ( $n = 36$ ). Fifty-six percent of intertidal flats had macroalgal cover above zero but less than 30%, and only three out of the 36 sites sampled had macroalgal cover greater than 50%. Macroalgae were most abundant when water-residence time was moderate to long, mudflat topography was intermediate between smooth and hummocky, elevation was lower than 0 m above msl, and the median sediment grain size was around  $80 \mu\text{m}$ .

### Linear models to predict macroalgal abundance

We evaluated 28 linear models predicting macroalgal abundance (percent cover) using the full data set. Of the 28 models, half used  $\tau_c$  and half used  $\tau_d$ , so that 14 unique combinations of variables and interactions were tested once using  $\tau_c$ , and then the models were run again with the only change a switch to  $\tau_d$ . We compared these paired models (identical other than including either  $\tau_c$  or  $\tau_d$ ) and concluded that  $\tau_d$  was always better based on  $AIC_C$ . The six best models using  $\tau_d$  were selected for testing on the data restricted to macroalgal cover  $< 30\%$ . The top models all included  $\tau_d$  as a main effect, and this variable had the strongest main effect in almost all models (Fig. 7; Table 3). Macroalgal cover differed between  $\tau_d$  groups (ANOVA:  $F_{2,33} = 4.83$ ,  $p = 0.015$ ). Post hoc analyses revealed that macroalgal cover was higher on intermediate  $\tau_d$  flats (mean = 27% cover  $\pm 7$  SE) than hummocky flats (mean = 6% cover  $\pm 3$  SE), but that macroalgal abundance on smooth flats (15% cover  $\pm 4$  SE) was similar to hummocky and intermediate flats (Fig. 7). However, the interaction between flow-related variables and  $\tau_d$  in models complicates the interpretation of this main effect (Fig. 8). Mudflat topography can provide coarse estimates of macroalgal abundance, but predictions are better when nonlinearity is accounted for using interactions with fetch and residence time (Figs. 7, 8; Table 3).

Three of the best four models included an interaction between residence time and  $\tau_d$  (Figs. 8, 9; Table 3). The interaction indicated that macroalgal abundance increases with higher residence times on smooth flats, but decreases with higher residence times on hummocky flats (Fig. 8; Table 3). We explored the interaction with separate regressions between residence time and macroalgal cover for each topographic group. To meet model assumptions, we used generalized least squares, or ordinary least squares, as needed (details in Supporting Information). The relationship between residence time and macroalgae was significant for smooth sites ( $F_{1,10} = 12.3$ ,  $\beta_{\text{res}} = 0.2$ ,  $p = 0.01$ ), but was not for the intermediate sites ( $F_{1,11} = 0.9$ ,  $\beta_{\text{res}} = -0.4$ ,  $p = 0.4$ ). The test for hummocky flats exhibited some heteroscedasticity that was not fully corrected using generalized least squares, but parameter estimates and statistical tests still suggested a strong trend (Supporting Information,  $F_{1,9} = 14.2$ ,  $\beta_{\text{res}} = -0.2$ ,  $p < 0.01$ ). For an increase in residence time from 20 to 200 h, the interaction model predicts a 7% increase in macroalgal cover on smooth flats, but a 15% decrease on hummocky flats over the same interval. We also explored the interaction by excluding sites with short residence times ( $< 100$  h), and retesting the relationship between macroalgal abundance and mudflat topography using  $\tau_c$  (Supporting Information). There was a significant negative relationship between macroalgal abundance and  $\tau_c$  after excluding short water residence sites ( $F_{1,28} = 46.4$ ,  $\beta_{\tau} = -0.6$ ,  $p < 0.001$ ) (Supporting Information Fig. S7).

The best four Full-models were not different from each other based on  $AIC_C$ ; with the largest difference only  $\Delta AIC_C = 2.06$  (Table 3). The models all included  $\tau_d$ , and three

out of the four included the interaction between  $\tau_d$  and residence time (Table 3). Since the four models were relatively similar, we present results for the one example, Full-D, which included a residence time- $\tau_d$  interaction and elevation. The Full-D model had a RMSE of 18% cover, and  $R^2 = 0.48$  (Table 3; Fig. 9). The Low Cover-models (for data where coverage < 30%) were more easily distinguished based on  $AIC_C$ , with the smallest difference  $\Delta AIC_C = 3.83$  (Table 3). Predictive accuracy increased for Low Cover-models over Full models. The best Low Cover-model, Low Cover-D, included the residence time- $\tau_d$  interaction and elevation, had RMSE of 8% cover, and  $R^2 = 0.68$  (Table 3; Fig. 9).

Both Full and Low Cover models underpredicted cases of high coverage on flats. The maximum macroalgal cover predicted from any of the Full models was 37%, and in the Low Cover models the highest cover predicted was 15%. Since macroalgal cover was right skewed, this limitation did not compromise prediction too severely. Only four out of 36 sites in the Full data set had macroalgal cover greater than 37%, and only three out of 26 sites had macroalgal cover greater than 15% in the Low Cover data set. The importance of elevation increased in the Low Cover models. Elevation was not significant for the Full-D ( $\beta_{\text{elev}} = -0.35$ ,  $p = 0.11$ ), but was for Low Cover-D where elevation was highly significant ( $\beta_{\text{elev}} = -0.50$ ,  $p = 0.001$ ) (Table 3).

We validated the Full models against data collected in 2015 and 2016 (Table 3). We could not validate the Low Cover models with these data, because high cover sites were overrepresented in this small validation data set (cover > 15% for 42% of measurements). These models back-predicted cover well (correlations = 0.87 or above, RMSE = 0.08 or less, Table 3). Based on these tests, Full-A, Full-C, and Full-D had similar prediction accuracy, with Full-B performing slightly less well (Table 3).

## Discussion

Despite understanding of mechanisms driving macroalgal accumulation, prediction of abundance across a range of environmental conditions and at different spatial scales remains poor. In this study, we explored hydrologic and geomorphic predictors of macroalgal distributions on intertidal flats in shallow, soft-sediment lagoons. The Virginia Coast Reserve was a good test system for physical parameters because other factors affecting macroalgal distribution (e.g., nutrients, herbivory) do not vary between sites, and can serve as a baseline predictor upon which to add other cofactors in systems where they may be important. Using high-resolution LiDAR data, we developed a novel index variable of mudflat topographic variation that was a useful predictor of macroalgal distribution. Macroalgal abundance was lower on hummocky tidal flats than smoother flats. Predictions of macroalgal abundance were improved after accounting for interactions between mudflat topography and water residence time. These interactions

improved models by explaining higher macroalgal abundances than expected on hummocky flats and lower than expected on smooth flats. These results suggest macroalgal distribution and abundance can be successfully modeled over large seascape areas using a simple set of flow-related and geomorphic variables.

## Mudflat topography quantification and drivers

The geomorphology of intertidal flats is controlled by feedbacks among biological, hydrologic, and geologic factors (Fagherazzi et al. 2007, 2013; Weerman et al. 2010). However, a metric to quantify or categorize mudflat topography has yet to be developed, limiting comparisons across flats in coastal lagoons. The topographic index variable we developed successfully differentiated flats in relation to macroalgal abundance. Percent clay was positively related to the mudflat topographic index, with higher clay corresponding with the formation of hummocks. The cohesive properties of clay bind sediments when content is at least 10% (van Ledden et al. 2004), possibly facilitating the building of hummocks. All of the sites in the hummocky category had greater than 10% clay, and clay content was significantly higher on hummocky flats than smooth or intermediate flats (Table 2). Some smooth and intermediate flats also had high clay content, indicating clay is not the only driver of mudflat topography on flats. Nevertheless, clay was a good predictor of mudflat topography across a wide range of environmental conditions.

Factors other than clay, residence time, and fetch, should affect mudflat topography, such as biological processes, total sediment delivery, and water depth. Biofilm formation (Weerman et al. 2010; Reidenbach and Timmerman 2019), bioturbation (Woodin 1978; Widdows and Brinsley 2002; Fagherazzi et al. 2013), and oyster reefs (McGlathery et al. 2013; Wiberg et al. 2019) could all contribute to mudflat topographic patterns by affecting sediment dynamics and erodibility. We observed mudflat topographic variation on smooth flats in the field; however, these formations were within the error for LiDAR data (< 6 cm in the vertical direction). Mudflat topographic variation on this scale is similar to patterns caused by biofilm and macrofauna (Woodin 1978; Widdows and Brinsley 2002; Weerman et al. 2010), suggesting mudflat topography on smooth flats may have been biologically driven (Widdows and Brinsley 2002; Weerman et al. 2010). On some flats, hummocks were colonized with narrow bands of oyster reef, suggesting a positive correlation between hummock development and oyster reef formation. Tidal flat geomorphic development is limited by wind waves that erode and scour sediments (Fagherazzi et al. 2007, 2013; McGlathery et al. 2013). As a result, we expected that higher fetch would relate to larger waves that may erode mudflat topographic features. We did not observe this pattern, and were surprised that SEM results indicated fetch did not explain mudflat topographic variation beyond its effect on clay content. Properly accounting for the effects of organisms, and other variables on

the building and maintenance of hummocks may improve the prediction of mudflat topography.

### Macroalgal distribution predicted by mudflat topography

The abundance of macroalgae on intertidal flats in the VCR is moderate as compared with other estuaries (Freshwater et al. 2006; Lyons et al. 2009; Byers et al. 2012; Sutula et al. 2014), and spatial patterns are related to *Diopatra cuprea* distributions (Thomsen and McGlathery 2005). *D. cuprea* are important for macroalgae in soft-sediment systems as they stabilize thalli and retain algae in the photic zone. In the VCR, macroalgal abundance and *D. cuprea* densities have been assessed across the mainland-barrier island gradient. Both are widespread, but macroalgae were found to be most abundant on mid-lagoon flats (130 g dw m<sup>-2</sup>) (Thomsen et al. 2006), and *D. cuprea* most abundant on mainland intertidal mudflats (35–40 tubes m<sup>-2</sup>) (Thomsen and McGlathery 2005). *D. cuprea* facilitates macroalgal accumulation across this mainland-barrier island gradient, with 70% of macroalgal thalli incorporated into *D. cuprea* tubes on mudflats (Thomsen and McGlathery 2005). By including mudflat topography in spatial distribution models macroalgae can be assessed at higher resolution over larger areas than previously possible, in part because topography relates to *D. cuprea* distributions. Both mudflat topography and *D. cuprea* are directly correlated with sediment grain size (Fig. 6), and indirectly with water residence time through its effect on sediment grain size (Wiberg et al. 2015). *D. cuprea* is most abundant in fine sands (Woodin 1978; Luckenbach 1986), and near the mainland, but resolving their distribution at a finer scale is difficult without intensive field sampling. We have observed mudflats with abundant *D. cuprea*, but without significant macroalgal accumulation, further indicating additional factors such as geomorphology and hydrology are important. Mudflat topography integrates multiple factors that affect macroalgal accumulation and growth, and might indicate *D. cuprea* density, making it a highly useful predictive metric.

Mudflat topography was a useful predictor of macroalgal abundance on intertidal flats; specifically, increased hummocks were negatively related to macroalgal abundance. One reason this pattern emerged was because mudflat topography integrates numerous environmental factors, such as *D. cuprea* distributions, sediment grain sizes, and tidal flat elevation. On average, hummocky sites in the VCR were higher in elevation than smooth or intermediate sites (Table 2). Macroalgae have poorer survival at high elevations where desiccation and heat stress are higher (Thomsen and McGlathery 2007; Thomsen et al. 2009). Macroalgae rapidly desiccate at elevations equal to or greater than 0 m above msl, and many hummocky flats were near or above this elevation (Thomsen and McGlathery 2007). When high macroalgal abundance sites (> 30% cover) were excluded, elevation became even more important in the models (Fig. 9; Table 3), further suggesting

low macroalgal abundance and absence was caused by stress at high elevations.

Mudflat topography also likely integrated some of the variability in flow-related variables, which affects macroalgal abundance through algal advection, and mass transport of dissolved gases and nutrients at both the tidal flat scale and across thalli surfaces (Jørgensen and Revsbech 1985; Flindt et al. 1997; Sand-Jensen and Frost-Christensen 1999). Most hummocky flats occurred in higher residence-time locations. Their complex bed topography may also have further slowed water velocity (McGlathery et al. 2013). Extremely thick diffusive boundary layers could form in these conditions, limiting gas and nutrient uptake and inhibiting growth (Jørgensen and Revsbech 1985). Additionally, the higher elevations of hummocky flats sometimes resulted in steeper slopes between subtidal areas and the flat platform, which could limit advective transport of macroalgae onto the flat (Salomonsen et al. 1997; Lanari and Copertino 2017). Macroalgal thalli that did accumulate on hummocky flats usually were found in hollows, or low-elevation channels between hummocks (with the exception of hummocky flats in lagoon units with water residence times < 100 h, discussed in greater detail below). These channels often did not fully drain during low tide, with 2–6 cm of standing water remaining. Shallow pools in channels could get very hot and possibly depleted of oxygen at low tide. While we did not measure channel conditions at low tide, we observed the thalli that accumulated in hummock channels were in various stages of decay. As a result of elevation and feedbacks between mudflat topography and flow conditions, macroalgae were usually not able to establish in high abundance on flats with more hummocky mudflat topography.

### Mudflat topography and water residence time interaction

The relationship between macroalgal abundance and mudflat topography ( $\tau_c$ ) for sites with water residence times greater than 100 h was strongly negative (Supporting Information). This suggests that for most tidal flats topography is a good predictor of macroalgal abundance, with macroalgae decreasing as hummocks increase. However, exceptions to this pattern occurred with short water residence times. Because of this, including an interaction term between mudflat topography and water residence time significantly improved models.

The pattern of higher macroalgal abundance on smoother tidal flats reversed with short water residence times (< 100 h) (Fig. 8). Smooth flats at short residence times had unusually low macroalgal abundances (including two sites without any macroalgae). These sites were dominated by sands, almost completely devoid of fine sediments, were near an inlet, and highly exposed. High disturbance from waves and high current speeds on these smooth, exposed flats may lead to macroalgal advection off the tidal flat, and prevent macroalgae stabilizing and accumulating (Flindt et al. 1997; Salomonsen et al. 1997; Lanari and Copertino 2017). While typically smooth mudflat topography promoted macroalgal

accumulation, in areas with high water velocities the lack of sheltering topographic relief prevented accumulation.

Hummocky sites with short water residence times (< 100 h) had higher macroalgal abundance than other hummocky sites. We hypothesize hummocky flats with higher than typical macroalgal abundances were the result of geomorphic features that formed small (~ 1 ha), locally sheltered flats, within lagoon units (~ 7 ha) characterized by short water residence times and fast-moving waters. This cross-scale interaction could promote fine sediment and macroalgal settlement over tidal flats, while tidal flushing in the larger lagoon unit refreshed oxygen and nutrient supply, thereby avoiding the physical and biological factors limiting macroalgae over typical hummocky flats. In streams, the presence of side channels, backwaters, and/or isolated pools cause small reaches to exhibit locally long residence times with restricted hydrologic exchange with the main channel, so that particulates, fine sediments, algae, and other organisms accumulate (Reynolds et al. 1991; Gooseff et al. 2007). Hummocky sites (usually containing higher clay content, Table 2), within short water residence time areas (usually lower clay, Fig. 2) (Wiberg et al. 2015), may suggest the presence of high retention side pools, or “transient storage” areas, as in streams (Reynolds et al. 1991; Gooseff et al. 2007). The transient storage area is still flushed by the channel, but at a slower rate than adjacent regions, promoting both entrapment and growth of macroalgae (Gooseff et al. 2007).

We do not know how ubiquitous these muddy- “side pool,” or exposed-sandy tidal flats are throughout coastal-barrier systems like the VCR. But together, these short water residence time cases suggest that there is a threshold effect of mudflat topography. Specifically, we hypothesize hummocks have a negative effect on macroalgal growth and accumulation, except when water residence times in lagoon units are less than 100 h, at which point the hummocky features help stabilize macroalgae. In these fast-moving waters, hummocks have a positive effect, sheltering macroalgae from advective transport off flats.

### Model limitations

Due to our limited sample size ( $n = 36$  tidal flats), we were unable to use cross-validation and most of the models had moderate  $R^2$  values (i.e.,  $R^2$  mainly < 0.5 with the exception of Low Cover-D for which  $R^2 = 0.68$ , Table 3, Fig. 9). However, the models predicted algal coverage well for independent data collected in other years (Table 3). In addition, they point to a set of physical parameters that to date have not been included in models of macroalgal abundance and distribution. Across the three Low Cover and three Full model formulations that included mudflat topography and residence time, parameter estimates were consistent in direction and similar in magnitude. These models, developed from field surveys, provide first-order predictions that may be improved with future field testing and validation, ideally over a wider range of conditions

than studied here and over multiple time points. For example, future research should predict macroalgal cover in the field using this suite of models, then survey macroalgae to estimate model precision and accuracy. These results will help to identify the most important predictors of macroalgal abundance and provide a basis for mechanistic hypotheses.

Additional factors should also be considered. For example, the relationship between *D. cuprea* and macroalgal abundance is well established (Thomsen and McGlathery 2005; Kollars et al. 2016), and may help explain distributions in addition to physical variables. Since directly measuring polychaete abundance is at least as intensive as monitoring macroalgae directly, the topographic index we developed can advance prediction of macroalgae over large spatial areas, like the > 900 km<sup>2</sup> VCR LTER. However, model accuracy declined when macroalgal cover was above 30%. *D. cuprea* density and distribution might explain macroalgal abundances greater than 30% cover, and their inclusion in statistical models could improve macroalgal prediction in these cases. Positive feedbacks may also explain abundances > 30% cover, resulting from distinct macroalgal patches overlapping, and forming a homogenous mat. This process promotes macroalgal mat stability, and resistance to erosive forces from waves (Lawson et al. 2012; Volaric et al. 2019). Even with these limitations, a novel mudflat topographic index, that can be measured with remote sensing, along with hydrological features is a promising predictor of macroalgal abundance on large spatial scales appropriate for monitoring.

### Conclusions

Analysis of macroalgal distribution and abundance using topographic indices is promising, because this approach may allow better resolution of algal impacts on coastal ecosystems over large spatial scales. The patchy distribution of depth, substrate-type, vegetation, and other variables in shallow lagoons has complicated the modeling of processes over large spatial extents. The interaction between mudflat topography and water residence time helped explain macroalgal abundance in this study indicating the possibility of better prediction of macroalgae over spatial scales relevant for ecosystem studies. These models also indicate how physical factors determine macroalgal colonization, survival, growth, and proliferation to high abundances.

Changes in macroalgal dynamics due to overfishing, eutrophication, and species invasions are having large impacts on coastal ecosystems worldwide (Mumby 2006; McGlathery et al. 2007; Williams and Smith 2007). This work shows that activities impacting coastal flow and circulation, sediment delivery, and bathymetry affect macroalgae and consequently ecosystem function. Accelerations of shoreline hardening, dredging, damming, and coastal development are occurring globally (Syvitski 2008; Bulleri and Chapman 2010; Temmerman et al. 2013). Thus, in addition to the better-

known drivers affecting macroalgae like eutrophication, physical processes also require study. By identifying models that predict macroalgal density at hectare and greater spatial scales across coastal seascapes, understanding of both local and global change processes affecting coastal ecosystems can be improved.

## References

- Anderson, I., C. Tobias, B. Neikirk, and R. Wetzel. 1997. Development of a process-based nitrogen mass balance model for a Virginia (USA) *Spartina alterniflora* salt marsh: Implications for net DIN flux. *Mar. Ecol. Prog. Ser.* **159**: 13–27. doi:[10.3354/meps159013](https://doi.org/10.3354/meps159013)
- Anderson, I., J. Stanhope, A. Hardison, and K. McGlathery. 2010. Sources and fates of nitrogen in Virginia coastal bays, p. 43–72. *In* M. Kennish and H. Paerl [eds.], *Coastal lagoons*. CRC Press.
- Arnold, T. W. 2010. Uninformative parameters and model selection using Akaike's information criterion. *J Wildl Manag* **74**: 1175–1178. doi:[10.1111/j.1937-2817.2010.tb01236.x](https://doi.org/10.1111/j.1937-2817.2010.tb01236.x)
- Besterman, A. F., and M. L. Pace. 2018. Do macroalgal mats impact microphytobenthos on mudflats? Evidence from a meta-analysis, comparative survey, and large-scale manipulation. *Estuaries Coast.* **41**: 2304–2316. doi:[10.1007/s12237-018-0418-3](https://doi.org/10.1007/s12237-018-0418-3)
- Bulleri, F., and M. G. Chapman. 2010. The introduction of coastal infrastructure as a driver of change in marine environments. *J. Appl. Ecol.* **47**: 26–35. doi:[10.1111/j.1365-2664.2009.01751.x](https://doi.org/10.1111/j.1365-2664.2009.01751.x)
- Burkepile, D. E., and M. E. Hay. 2006. Herbivore vs. nutrient control of marine primary producers: Context-dependent effects. *Ecology* **87**: 3128–3139. doi:[10.1890/0012-9658\(2006\)87\[3128:HVNCOM\]2.0.CO;2](https://doi.org/10.1890/0012-9658(2006)87[3128:HVNCOM]2.0.CO;2)
- Burnham, K. P., and D. R. Anderson. 1998. *Model selection and inference: A practical information-theoretic approach*. Springer-Verlag.
- Burnham, K. P., D. R. Anderson, and K. P. Huyvaert. 2011. AIC model selection and multimodel inference in behavioral ecology: Some background, observations, and comparisons. *Behav. Ecol. Sociobiol.* **65**: 23–35. doi:[10.1007/s00265-010-1029-6](https://doi.org/10.1007/s00265-010-1029-6)
- Byers, J. E., P. E. Gribben, C. Yeager, and E. E. Sotka. 2012. Impacts of an abundant introduced ecosystem engineer within mudflats of the southeastern US coast. *Biol. Invasions* **14**: 2587–2600. doi:[10.1007/s10530-012-0254-5](https://doi.org/10.1007/s10530-012-0254-5)
- Cloern, J. E. 2001. Our evolving conceptual model of the coastal eutrophication problem. *Mar. Ecol. Prog. Ser.* **210**: 223–253. doi:[10.3354/meps210223](https://doi.org/10.3354/meps210223)
- Cox, T. E., H. L. Spalding, and M. S. Foster. 2017. Spatial and temporal variation of diverse inter-tidal algal assemblages in Southwest O'ahu. *Mar. Ecol.* **38**: e12429. doi:[10.1111/maec.12429](https://doi.org/10.1111/maec.12429)
- Dahl, A. L. 1973. Surface area in ecological analysis: Quantification of benthic coral-reef algae. *Mar. Biol.* **23**: 239–249. doi:[10.1007/BF00389331](https://doi.org/10.1007/BF00389331)
- Dewberry. 2016. Eastern Shore Virginia QL2 LiDAR BAA: Report produced for U.S. Geological Survey. Task Order: G15PD00284. Task Order: G15PD00284.
- Fagherazzi, S., C. Palermo, M. C. Rulli, L. Carniello, and A. Defina. 2007. Wind waves in shallow microtidal basins and the dynamic equilibrium of tidal flats. *J. Geophys. Res.* **112**: F02024. doi:[10.1029/2006JF000572](https://doi.org/10.1029/2006JF000572)
- Fagherazzi, S., and others. 2013. Ecogeomorphology of tidal flats, p. 201–220. *In* J. F. Shroder [ed.], *Ecogeomorphology. Treatise on geomorphology*. Academic Press.
- Ferguson, A. E. 2018. Evaluating nature-based solutions to storm wave impacts in the Virginia Coast Reserve. M.S. thesis. Univ. of Virginia.
- Flindt, M., J. Salomonsen, M. Carrer, M. Bocci, and L. Kamp-Nielsen. 1997. Loss, growth and transport dynamics of *Chaetomorpha aerea* and *Ulva rigida* in the Lagoon of Venice during an early summer field campaign. *Ecol. Model.* **102**: 133–141. doi:[10.1016/S0304-3800\(97\)00093-8](https://doi.org/10.1016/S0304-3800(97)00093-8)
- Freshwater, D. W., J. K. Greene, R. M. Hamner, and F. Montgomery. 2006. Seasonality of the invasive seaweed *Gracilaria vermiculophylla* along the southeastern coast of North Carolina. *J. N. C. Acad. Sci.* **122**: 49–55. doi:[10.2307/24336115](https://doi.org/10.2307/24336115)
- Ganju, N. K., S. E. Suttles, A. Beudin, D. J. Nowacki, J. L. Miselis, and B. D. Andrews. 2017. Quantification of storm-induced bathymetric change in a back-barrier estuary. *Estuaries Coast.* **40**: 22–36. doi:[10.1007/s12237-016-0138-5](https://doi.org/10.1007/s12237-016-0138-5)
- Giordano, J. C. P., M. J. Brush, and I. C. Anderson. 2011. Quantifying annual nitrogen loads to Virginia's coastal lagoons: Sources and water quality response. *Estuaries Coast.* **34**: 297–309. doi:[10.1007/s12237-010-9345-7](https://doi.org/10.1007/s12237-010-9345-7)
- Gonzalez, D. J., A. R. Smyth, M. F. Piehler, and K. J. McGlathery. 2013. Mats of the nonnative macroalga, *Gracilaria vermiculophylla*, alter net denitrification rates and nutrient fluxes on intertidal mudflats. *Limnol. Oceanogr.* **58**: 2101–2108. doi:[10.4319/lo.2013.58.6.2101](https://doi.org/10.4319/lo.2013.58.6.2101)
- Gooseff, M. N., R. O. Hall, and J. L. Tank. 2007. Relating transient storage to channel complexity in streams of varying land use in Jackson Hole, Wyoming. *Water Resour. Res.* **43**: W01417. doi:[10.1029/2005WR004626](https://doi.org/10.1029/2005WR004626)
- Gosner, K. L. 1971. *Guide to identification of marine and estuarine invertebrates: Cape Hatteras to the Bay of Fundy*. John Wiley.
- Grace, J. B., T. M. Anderson, H. Olf, and S. M. Scheiner. 2010. On the specification of structural equation models for ecological systems. *Ecol. Monogr.* **80**: 67–87. doi:[10.1890/09-0464.1](https://doi.org/10.1890/09-0464.1)
- Green, L., and P. Fong. 2016. The good, the bad and the *Ulva*: The density dependent role of macroalgal subsidies in influencing diversity and trophic structure of an

- estuarine community. *Oikos* **125**: 988–1000. doi:[10.1111/oik.02860](https://doi.org/10.1111/oik.02860)
- Greiner, J. T., K. J. McGlathery, J. Gunnell, and B. A. McKee. 2013. Seagrass restoration enhances “blue carbon” sequestration in coastal waters. *PLoS One* **8**: e72469. doi:[10.1371/journal.pone.0072469](https://doi.org/10.1371/journal.pone.0072469)
- Guillemin, M.-L., S. Faugeton, C. Destombe, F. Viard, J. A. Correa, and M. Valero. 2008. Genetic variation in wild and cultivated populations of the haploid-diploid red alga *Gracilaria chilensis*: How farming practices favor asexual reproduction and heterozygosity. *Evolution* **62**: 1500–1519. doi:[10.1111/j.1558-5646.2008.00373.x](https://doi.org/10.1111/j.1558-5646.2008.00373.x)
- Gulbransen, D. J., K. J. McGlathery, M. Marklund, J. N. Norris, and C. F. D. Gurgel. 2012. *Gracilaria vermiculophylla* (Rhodophyta, Gracilariales) in the Virginia coastal bays, USA: COX1 analysis reveals high genetic richness of an introduced macroalga. *J. Phycol.* **48**: 1278–1283. doi:[10.1111/j.1529-8817.2012.01218.x](https://doi.org/10.1111/j.1529-8817.2012.01218.x)
- Gurgel, C. F. D., J. N. Norris, W. E. Schmidt, H. N. Le, and S. Fredericq. 2018. Systematics of the Gracilariales (Rhodophyta) including new subfamilies, tribes, subgenera, and two new genera, *Agarophyton gen. nov.* and *Crassa gen. nov.* *Phytotaxa* **374**: 1. doi:[10.11646/phytotaxa.374.1.1](https://doi.org/10.11646/phytotaxa.374.1.1)
- Hardison, A. K., I. C. Anderson, E. A. Canuel, C. R. Tobias, and B. Veuger. 2011. Carbon and nitrogen dynamics in shallow photic systems: Interactions between macroalgae, microalgae, and bacteria. *Limnol. Oceanogr.* **56**: 1489–1503. doi:[10.4319/lo.2011.56.4.1489](https://doi.org/10.4319/lo.2011.56.4.1489)
- Hartigan, J. A., and M. A. Wong. 1979. Algorithm AS 136: A k-means clustering algorithm. *J. R. Stat. Soc.* **28**: 100–108. doi:[10.2307/2346830](https://doi.org/10.2307/2346830)
- Holmes, K. W., K. P. Van Niel, B. Radford, G. A. Kendrick, and S. L. Grove. 2008. Modelling distribution of marine benthos from hydroacoustics and underwater video. *Cont. Shelf Res.* **28**: 1800–1810. doi:[10.1016/j.csr.2008.04.016](https://doi.org/10.1016/j.csr.2008.04.016)
- Jørgensen, B. B., and N. P. Revsbech. 1985. Diffusive boundary layers and the oxygen uptake of sediments and detritus: Diffusive boundary layers. *Limnol. Oceanogr.* **30**: 111–122. doi:[10.4319/lo.1985.30.1.0111](https://doi.org/10.4319/lo.1985.30.1.0111)
- Kain(Jones), J. M., and C. Destombe. 1995. A review of the life history, reproduction and phenology of *Gracilaria*. *J. Appl. Phycol.* **7**: 269–281. doi:[10.1007/BF00004001](https://doi.org/10.1007/BF00004001)
- Kollars, N., J. Byers, and E. Sotka. 2016. Invasive décor: An association between a native decorator worm and a non-native seaweed can be mutualistic. *Mar. Ecol. Prog. Ser.* **545**: 135–145. doi:[10.3354/meps11602](https://doi.org/10.3354/meps11602)
- Kotta, J., and others. 2019. Integrating experimental and distribution data to predict future species patterns. *Sci. Rep.* **9**: 1821. doi:[10.1038/s41598-018-38416-3](https://doi.org/10.1038/s41598-018-38416-3)
- Krause-Jensen, D., A. L. Middelboe, J. Carstensen, and K. Dahl. 2007. Spatial patterns of macroalgal abundance in relation to eutrophication. *Mar. Biol.* **152**: 25–36. doi:[10.1007/s00227-007-0676-2](https://doi.org/10.1007/s00227-007-0676-2)
- Krueger-Hadfield, S. A., and others. 2016. Invasion of novel habitats uncouples haplo-diplontic life cycles. *Mol. Ecol.* **25**: 3801–3816. doi:[10.1111/mec.13718](https://doi.org/10.1111/mec.13718)
- Krueger-Hadfield, S. A., and others. 2017. Genetic identification of source and likely vector of a widespread marine invader. *Ecol. Evol.* **7**: 4432–4447. doi:[10.1002/ece3.3001](https://doi.org/10.1002/ece3.3001)
- Lanari, M., and M. Copertino. 2017. Drift macroalgae in the Patos Lagoon Estuary (southern Brazil): Effects of climate, hydrology and wind action on the onset and magnitude of blooms. *Mar. Biol. Res.* **13**: 36–47. doi:[10.1080/17451000.2016.1225957](https://doi.org/10.1080/17451000.2016.1225957)
- Lawson, S., K. McGlathery, and P. Wiberg. 2012. Enhancement of sediment suspension and nutrient flux by benthic macrophytes at low biomass. *Mar. Ecol. Prog. Ser.* **448**: 259–270. doi:[10.3354/meps09579](https://doi.org/10.3354/meps09579)
- Lees, L. E., S. A. Krueger-Hadfield, A. J. Clark, E. A. Duermit, E. E. Sotka, and C. J. Murren. 2018. Nonnative *Gracilaria vermiculophylla* tetrasporophytes are more difficult to debranch and are less nutritious than gametophytes. *J. Phycol.* **54**: 471–482. doi:[10.1111/jpy.12746](https://doi.org/10.1111/jpy.12746)
- Lefcheck, J. S. 2016. piecewiseSEM: Piecewise structural equation modeling in R for ecology, evolution, and systematics. *Methods Ecol. Evol.* **7**: 573–579. doi:[10.1111/2041-210X.12512](https://doi.org/10.1111/2041-210X.12512)
- Luckenbach, M. W. 1986. Sediment stability around animal tubes: The roles of hydrodynamic processes and biotic activity: Stability around tubes. *Limnol. Oceanogr.* **31**: 779–787. doi:[10.4319/lo.1986.31.4.0779](https://doi.org/10.4319/lo.1986.31.4.0779)
- Lyons, P., C. Thornber, J. Portnoy, and E. Gwilliam. 2009. Dynamics of macroalgal blooms along the Cape Cod National Seashore. *Northeast. Nat.* **16**: 53–66. doi:[10.1656/045.016.0105](https://doi.org/10.1656/045.016.0105)
- Martínez, B., R. M. Viejo, F. Carreño, and S. C. Aranda. 2012. Habitat distribution models for intertidal seaweeds: Responses to climatic and non-climatic drivers: Distribution models for intertidal seaweeds in North-Western Iberia. *J. Biogeogr.* **39**: 1877–1890. doi:[10.1111/j.1365-2699.2012.02741.x](https://doi.org/10.1111/j.1365-2699.2012.02741.x)
- Martins, I., R. J. Lopes, A. I. Lillebø, J. M. Neto, M. A. Pardal, J. G. Ferreira, and J. C. Marques. 2007. Significant variations in the productivity of green macroalgae in a mesotidal estuary: Implications to the nutrient loading of the system and the adjacent coastal area. *Mar. Pollut. Bull.* **54**: 678–690. doi:[10.1016/j.marpolbul.2007.01.023](https://doi.org/10.1016/j.marpolbul.2007.01.023)
- McGlathery, K. J., I. C. Anderson, and A. C. Tyler. 2001. Magnitude and variability of benthic and pelagic metabolism in a temperate coastal lagoon. *Mar. Ecol. Prog. Ser.* **216**: 1–15. doi:[10.3354/meps216001](https://doi.org/10.3354/meps216001)
- McGlathery, K. J., K. Sundbäck, and I. C. Anderson. 2007. Eutrophication in shallow coastal bays and lagoons: The role of plants in the coastal filter. *Mar. Ecol. Prog. Ser.* **348**: 1–18. doi:[10.3354/meps07132](https://doi.org/10.3354/meps07132)
- McGlathery, K. J., K. Sundbäck, and P. Fong. 2012. Estuarine benthic algae, p. 203–234. *In* J. W. Day, B. C. Crump,

- W. M. Kemp, and A. Yáñez-Arancibia [eds.], *Estuarine ecology*. John Wiley & Sons.
- McGlathery, K. J., M. Reidenbach, P. D'Odorico, S. Fagherazzi, M. Pace, and J. Porter. 2013. Nonlinear dynamics and alternative stable states in shallow coastal systems. *Oceanography* **26**: 220–231. doi:[10.5670/oceanog.2013.66](https://doi.org/10.5670/oceanog.2013.66)
- McGlathery, K. J., and R. R. Christian. 2018. Water quality sampling - integrated measurements for the Virginia Coast, 1992–2018. Virginia Coast Reserve Long-Term Ecological Research Project Data Publication knb-lter-vcr.247.10. doi:[10.6073/pasta/b650b236f092e0fdee0d5d8ccf521cb3](https://doi.org/10.6073/pasta/b650b236f092e0fdee0d5d8ccf521cb3)
- Mumby, P. J. 2006. Fishing, trophic cascades, and the process of grazing on coral reefs. *Science* **311**: 98–101. doi:[10.1126/science.1121129](https://doi.org/10.1126/science.1121129)
- Murray, N. J., and others. 2019. The global distribution and trajectory of tidal flats. *Nature* **565**: 222–225. doi:[10.1038/s41586-018-0805-8](https://doi.org/10.1038/s41586-018-0805-8)
- Nejrup, L. B., and M. F. Pedersen. 2010. Growth and biomass development of the introduced red alga *Gracilaria vermiculophylla* is unaffected by nutrient limitation and grazing. *Aquat. Biol.* **10**: 249–259. doi:[10.3354/ab00281](https://doi.org/10.3354/ab00281)
- R Core Team. 2019. R: A language and environment for statistical computing. R Foundation for Statistical Computing.
- Reidenbach, M. A., and R. Timmerman. 2019. Interactive effects of seagrass and the microphytobenthos on sediment suspension within shallow coastal bays. *Estuaries Coast.* **42**: 2038–2053. doi:[10.1007/s12237-019-00627-w](https://doi.org/10.1007/s12237-019-00627-w)
- Reynolds, C. S., P. A. Carling, and K. J. Beven. 1991. Flow in river channels: New insights into hydraulic retention. *Arch. Hydrobiol.* **121**: 171–179.
- Rogers, J. S., S. A. Maticka, V. Chirayath, C. B. Woodson, J. J. Alonso, and S. G. Monismith. 2018. Connecting flow over complex terrain to hydrodynamic roughness on a coral reef. *J. Phys. Oceanogr.* **48**: 1567–1587. doi:[10.1175/JPO-D-18-0013.1](https://doi.org/10.1175/JPO-D-18-0013.1)
- Safak, I., P. L. Wiberg, D. L. Richardson, and M. O. Kurum. 2015. Controls on residence time and exchange in a system of shallow coastal bays. *Cont. Shelf Res.* **97**: 7–20. doi:[10.1016/j.csr.2015.01.009](https://doi.org/10.1016/j.csr.2015.01.009)
- Salomonsen, J., M. R. Flindt, and O. Geertz-Hansen. 1997. Significance of advective transport of *Ulva lactuca* for a biomass budget on a shallow water location. *Ecol. Model.* **102**: 129–132. doi:[10.1016/S0304-3800\(97\)00100-2](https://doi.org/10.1016/S0304-3800(97)00100-2)
- Sand-Jensen, K., and H. Frost-Christensen. 1999. Plant growth and photosynthesis in the transition zone between land and stream. *Aquat. Bot.* **63**: 23–35. doi:[10.1016/S0304-3770\(98\)00107-7](https://doi.org/10.1016/S0304-3770(98)00107-7)
- Snickars, M., M. Gullström, G. Sundblad, U. Bergström, A.-L. Downie, M. Lindgarth, and J. Mattila. 2014. Species–environment relationships and potential for distribution modelling in coastal waters. *J. Sea Res.* **85**: 116–125. doi:[10.1016/j.seares.2013.04.008](https://doi.org/10.1016/j.seares.2013.04.008)
- Stanhope, J. W., I. C. Anderson, and W. G. Reay. 2009. Base flow nutrient discharges from lower Delmarva Peninsula watersheds of Virginia, USA. *J. Environ. Qual.* **38**: 2070–2083. doi:[10.2134/jeq2008.0358](https://doi.org/10.2134/jeq2008.0358)
- Sutula, M., L. Green, G. Cicchetti, N. Detenbeck, and P. Fong. 2014. Thresholds of adverse effects of macroalgal abundance and sediment organic matter on benthic habitat quality in estuarine intertidal flats. *Estuaries Coast.* **37**: 1532–1548. doi:[10.1007/s12237-014-9796-3](https://doi.org/10.1007/s12237-014-9796-3)
- Swaney, D. P., D. Scavia, R. W. Howarth, and R. M. Marino. 2008. Estuarine classification and response to nitrogen loading: Insights from simple ecological models. *Estuar. Coast. Shelf Sci.* **77**: 253–263. doi:[10.1016/j.ecss.2007.09.013](https://doi.org/10.1016/j.ecss.2007.09.013)
- Syvitski, J. P. M. 2008. Deltas at risk. *Sustain. Sci.* **3**: 23–32. doi:[10.1007/s11625-008-0043-3](https://doi.org/10.1007/s11625-008-0043-3)
- Temmerman, S., P. Meire, T. J. Bouma, P. M. J. Herman, T. Ysebaert, and H. J. De Vriend. 2013. Ecosystem-based coastal defence in the face of global change. *Nature* **504**: 79–83. doi:[10.1038/nature12859](https://doi.org/10.1038/nature12859)
- Thomsen, M. S., C. F. D. Gurgel, S. Fredericq, and K. J. McGlathery. 2005. *Gracilaria vermiculophylla* (Rhodophyta, Gracilariales) in Hog Island Bay, Virginia: A cryptic alien and invasive macroalga and taxonomic correction. *J. Phycol.* **42**: 139–141. doi:[10.1111/j.1529-8817.2005.00160.x](https://doi.org/10.1111/j.1529-8817.2005.00160.x)
- Thomsen, M. S., and K. J. McGlathery. 2005. Facilitation of macroalgae by the sedimentary tube forming polychaete *Diopatra cuprea*. *Estuar. Coast. Shelf Sci.* **62**: 63–73. doi:[10.1016/j.ecss.2004.08.007](https://doi.org/10.1016/j.ecss.2004.08.007)
- Thomsen, M. S., K. J. McGlathery, and A. C. Tyler. 2006. Macroalgal distribution patterns in a shallow, soft-bottom lagoon, with emphasis on the nonnative *Gracilaria vermiculophylla* and *Codium fragile*. *Estuaries Coast.* **29**: 465–473. doi:[10.1007/BF02784994](https://doi.org/10.1007/BF02784994)
- Thomsen, M. S., and K. J. McGlathery. 2007. Stress tolerance of the invasive macroalgae *Codium fragile* and *Gracilaria vermiculophylla* in a soft-bottom turbid lagoon. *Biol. Invasions* **9**: 499–513. doi:[10.1007/s10530-006-9043-3](https://doi.org/10.1007/s10530-006-9043-3)
- Thomsen, M. S., K. J. McGlathery, A. Schwarzschild, and B. R. Silliman. 2009. Distribution and ecological role of the non-native macroalga *Gracilaria vermiculophylla* in Virginia salt marshes. *Biol. Invasions* **11**: 2303–2316. doi:[10.1007/s10530-008-9417-9](https://doi.org/10.1007/s10530-008-9417-9)
- Tyler, A. C., K. J. McGlathery, and I. C. Anderson. 2003. Benthic algae control sediment: Water column fluxes of organic and inorganic nitrogen compounds in a temperate lagoon. *Limnol. Oceanogr.* **48**: 2125–2137. doi:[10.4319/lo.2003.48.6.2125](https://doi.org/10.4319/lo.2003.48.6.2125)
- Umanzor, S., L. Ladah, L. E. Calderon-Aguilera, and J. A. Zertuche-González. 2019. Testing the relative importance of intertidal seaweeds as ecosystem engineers across tidal heights. *J. Exp. Mar. Biol. Ecol.* **511**: 100–107. doi:[10.1016/j.jembe.2018.11.008](https://doi.org/10.1016/j.jembe.2018.11.008)
- Valiela, I., J. McClelland, J. Hauxwell, P. J. Behr, D. Hersh, and K. Foreman. 1997. Macroalgal blooms in shallow estuaries:

- Controls and ecophysiological and ecosystem consequences. *Limnol. Oceanogr.* **42**: 1105–1118. doi:[10.4319/lo.1997.42.5\\_part\\_2.1105](https://doi.org/10.4319/lo.1997.42.5_part_2.1105)
- van Ledden, M., W. G. M. van Kesteren, and J. C. Winterwerp. 2004. A conceptual framework for the erosion behaviour of sand–mud mixtures. *Cont. Shelf Res.* **24**: 1–11. doi:[10.1016/j.csr.2003.09.002](https://doi.org/10.1016/j.csr.2003.09.002)
- Volaric, M., P. Berg, and M. Reidenbach. 2018. Oxygen metabolism of intertidal oyster reefs measured by aquatic eddy covariance. *Mar. Ecol. Prog. Ser.* **599**: 75–91. doi:[10.3354/meps12627](https://doi.org/10.3354/meps12627)
- Volaric, M. P., P. Berg, and M. A. Reidenbach. 2019. An invasive macroalga alters ecosystem metabolism and hydrodynamics on a tidal flat. *Mar. Ecol. Prog. Ser.* **628**: 1–16. doi:[10.3354/meps13143](https://doi.org/10.3354/meps13143)
- Weerman, E. J., J. van de Koppel, M. B. Eppinga, F. Montserrat, Q. Liu, and P. M. J. Herman. 2010. Spatial self-organization on intertidal mudflats through biophysical stress divergence. *Am. Nat.* **176**: E15–E32. doi:[10.1086/652991](https://doi.org/10.1086/652991)
- Wiberg, P. L., J. A. Carr, I. Safak, and A. Anutaliya. 2015. Quantifying the distribution and influence of non-uniform bed properties in shallow coastal bays: Non-uniform bed properties in coastal bays. *Limnol. Oceanogr.: Methods* **13**: 746–762. doi:[10.1002/lom3.10063](https://doi.org/10.1002/lom3.10063)
- Wiberg, P. L., S. R. Taube, A. E. Ferguson, M. R. Kremer, and M. A. Reidenbach. 2019. Wave attenuation by oyster reefs in shallow coastal bays. *Estuaries Coast.* **42**: 331–347. doi:[10.1007/s12237-018-0463-y](https://doi.org/10.1007/s12237-018-0463-y)
- Widdows, J., and M. Brinsley. 2002. Impact of biotic and abiotic processes on sediment dynamics and the consequences to the structure and functioning of the intertidal zone. *J. Sea Res.* **48**: 143–156. doi:[10.1016/S1385-1101\(02\)00148-X](https://doi.org/10.1016/S1385-1101(02)00148-X)
- Williams, S. L., and J. E. Smith. 2007. A global review of the distribution, taxonomy, and impacts of introduced seaweeds. *Annu. Rev. Ecol. Evol. Syst.* **38**: 327–359. doi:[10.1146/annurev.ecolsys.38.091206.095543](https://doi.org/10.1146/annurev.ecolsys.38.091206.095543)
- Woodin, S. A. 1978. Refuges, disturbance, and community structure: A marine soft-bottom example. *Ecology* **59**: 274–284. doi:[10.2307/1936373](https://doi.org/10.2307/1936373)
- Zuur, A., E. N. Ieno, N. Walker, A. A. Saveliev, and G. M. Smith. 2009. Mixed effects models and extensions in ecology with R. Springer.

### Acknowledgments

This work was supported by the Department of Environmental Sciences at the University of Virginia. Field and lab technical assistance was provided by J. Blaze, J. Cai, B. Duke, R. Flick, R. Fowler, D. Ortiz, and M. Palmer. We thank the staff of the UVA Anheuser-Busch Coastal Research Center, specifically: Donna Fauber, David Lee, and Steve Parker, as well as Meg Miller, for guidance on project design and methods and support. The Nature Conservancy, U.S. National Park Service, Virginia Marine Resource Commission, and private leaseholders E. Bell, R. Cherrix, H. Jones Jr., M. O’Neil, and G. Stratton provided access to field sites. Support for this study was provided by National Science Foundation grant to the Virginia Coast Reserve Long-Term Ecological Research project (DEB-1832221 and DEB-1237733); 4-VA, a collaborative partnership for advancing the Commonwealth of Virginia; and the National Science Foundation Graduate Research Fellowship Program (DDGE-1315231).

### Conflict of Interest

None declared.

Submitted 20 January 2020

Revised 01 July 2020

Accepted 04 August 2020

Associate editor: Bradley Eyre